

Article

# Fire Blight Disease Detection for Apple Trees: Hyperspectral Analysis of Healthy, Infected and Dry Leaves

Hubert Skoneczny \*, Katarzyna Kubiak, Marcin Spiralski, Jan Kotlarz , Artur Mikiciński and Joanna Puławska

Lukasiewicz Research Network—Institute of Aviation, Space Technologies Center, Remote Sensing Division, 02–256 Warsaw, Poland; katarzyna.kubiak@ilot.lukasiewicz.gov.pl (K.K.); marcin.spiralski@ilot.lukasiewicz.gov.pl (M.S.); jan.kotlarz@ilot.lukasiewicz.gov.pl (J.K.); artur.mikicinski@inhort.pl (A.M.); joanna.pulawska@inhort.pl (J.P.)

\* Correspondence: hubert.skoneczny@ilot.lukasiewicz.gov.pl; Tel.: +48-609-708-704

Received: 19 May 2020; Accepted: 26 June 2020; Published: 30 June 2020



**Abstract:** The effective and rapid detection of Fire Blight, an important bacterial disease caused by the quarantine pest *E.amylovora*, is crucial for today’s horticulture. This study explored the application of non-invasive proximal hyperspectral remote sensing (RS) in order to differentiate the healthy (H), infected (I) and dry (D) leaves of apple trees. Analysis of variance was employed in order to determine which hyperspectral narrow spectral bands exhibited the most significant differences. Spectral signatures for the range of 400–2500 nm were acquired with Thermo Scientific Evolution 220 and iS50NIR spectrometers. The selected spectral bands were then used to evaluate several RS indices, including ARI (Anthocyanin Reflectance Index), RDVI (Renormalized Difference Vegetation Index), MSR (Modified Simple Ratio) and NRI (Nitrogen Reflectance Index), for Fire Blight detection in apple tree leaves. Furthermore, a new index was proposed, namely QFI. The spectral indices were tested on apple trees infected by Fire Blight in a quarantine greenhouse. Results indicated that the short-wavelength infrared (SWIR) band located at 1450 nm was able to distinguish (I) and (H) leaves, while the SWIR band at 1900 nm differentiated all three leaf types. Moreover, tests using the Pearson correlation indicated that ARI, MSR and QFI exhibited the highest correlations with the infection progress. Our results prove that our hyperspectral remote sensing technique is able to differentiate (H), (I) and (D) leaves of apple trees for the reliable and precise detection of Fire Blight.

**Keywords:** hyperspectral; spectroscopy in agriculture; fire blight detection; short wave infrared radiation; precision agriculture; remote sensing

## 1. Introduction

Poland ranks fourth in global apple production, with approximately 2.5 million tonnes produced annually, and over 800,000 tonnes of which are allocated for export. The Polish apple export market is estimated to have a value of €346 million. Pome fruit Fire Blight poses one of the greatest threats for the horticulture industry across the globe. Institutions such as the Main Inspectorate of Plant Health and Seed Inspection (MIPHI) in Poland have undertaken firm action on plant disease control. For example, in 2017, over 121,000 field inspections at agricultural entrepreneurs were performed on plant health and pathogen presence control throughout Poland. There is a great and indisputable need for research concerning Fire Blight detection on apple trees in order to develop rapid and precise methods that are able to reduce horticultural losses. In addition, the current detection method of onsite organoleptic assessments is considered obsolete, expensive, subjective, inaccurate and time-consuming. Thus, field inspectors are at present in need of an innovative approach.

Fire Blight is caused by the necrogenic Gram-negative bacterium *Erwinia amylovora*, which is considered as a quarantine organism and is subjected to compulsory control when detected on plant reproductive material. Due to its harmfulness, *E. amylovora* has been placed on the A2 EPPO quarantine list and its presence has been confirmed in 51 countries [1]. Furthermore, Fire Blight is considered as one of the most destructive bacterial diseases for apple (*Malus domestica*), pear (*Pyrus communis*) and, more generally, for Maloideae, a subfamily of the Rosaceae [2]. The pathogen enters the plant through natural openings such as nectarthodes or via wound locations on succulent aerial components of the plant. Once inside the susceptible host plant, the bacteria generally multiply in the apoplast of parenchyma cells and colonize active growing shoots, which subsequently induces the progressive necrosis of the infected plant tissues. In both resistant host and non-host plants, bacteria cause local cell death (via a hypersensitive-like reaction) and are unable to further colonize the plant tissue [3]. Typical symptoms of Fire Blight on apple trees include necrotic spots that develop on the margin of the leaf lamina or reddened petioles and the midrib of the leaves. The symptoms are similar among all stone fruit trees and are relatively easy to spot. Moreover, the name of the disease has its origins in its principle symptoms, namely the brownish appearance of sprouts, flowers and leaves, giving the impression of burning.

Fire Blight management can be divided into three key components: Prevention, reduction and eradication. Choosing orchard locations with unfavourable weather conditions for bacteria development, the employment of correct fertilization and irrigation procedures, suitable tree pruning and the prevention of off-season blooming can greatly ease the progress of the disease and reduce the chance of pathogens appearance [4]. If the Fire Blight was present in the previous season, management efforts should be directed in reducing the amount of bacteria inoculum before the bloom season. Copper compounds and antibiotics are the most commonly used bactericides in this case. However, authorities in numerous countries (including EU member states) have banned the use of antibiotics because of the potential risk of promoting the development of antibiotic resistance in human pathogens [5,6]. The spraying of copper-based bactericides during bud growth is a fairly effective preventive measure. However, it fails to heal plants already infected. Copper product ions kill bacteria and thus reduce their proliferation in cankers. This method significantly reduces bacteria dissemination via rain, wind and insects [7]. For the case of Fire Blight symptoms already visible in the orchard, the disease is eliminated for that season solely by eradicating all infected plant tissue. This is performed by the cutting the stems at approximately 35 cm below the visible symptoms [8].

Several significant studies relating to Fire Blight detection for different crop types were published at the turn of the past decade. Bagheri et al. (2018) [9] investigated the detection of Fire Blight in pear trees using the visible (VIS) and near-infrared (NIR) regions across the 380–1000-nm range. The hyperspectral differentiation of healthy (H), symptomatic (S) and non-symptomatic (MS) pear tree revealed the most useful spectral ranges (i.e., 541 nm (H), 522 nm (MS), 559 nm (S), 672 nm (H), 680 nm (MS) and 685 nm (S)), as well as the most promising Remote Sensing (RS) indices (i.e., SIPI—Structure Insensitive Pigment Index  $((R870-R570)/(R870-R670))$  and MSR—Modified Simple Ratio  $((R800/R670)-1)/\sqrt{((R800/R670)+1)}$ ) for Fire Blight detection.

Alnaasan (2015) [10] revealed the SWIR region (1350–1800 nm) to be the most effective spectrum range for early Fire Blight detection. This was attributed to the severe water stress caused by the pathogen. In addition, Jarolmasjed et al. (2019) [11] highlighted the superiority of hyperspectral data in capturing disease-specific responses for Fire Blight compared to VIS and multispectral imaging. The effective application of the VIS and NIR (325–1075 nm) spectral range for the monitoring of bacterial leaf blight disease in rice was demonstrated by Singh et al. (2012) [12], and in particular, the OSAVI (Optimized Soil Adjusted Vegetation Index) and RE (Red Edge) indices. Zhnag et al. (2004) [13] proposed three new RS indices for the detection of blight infection in tomato, namely D1  $((R800-R900)/(R600-R650)$  nm), D3  $((R800-R900)/(R2000-R2200)$  nm) and D4  $((R1000-R1100)/(R600-R650)$  nm)). The fusion of hyperspectral reflectance (HR) and nuclear magnetic resonance (NMR) was proved to be effective and affordable for the detection of *E.amylovora* infections by Rizzuto et al. (2018) [14] for pear leaves.

Most recently, Bagheri (2020) [15] conducted a more application-oriented study by evaluating the capability of multispectral remote sensing for Fire Blight detection in pear orchards. To analyse ground and aerial (obtained with unmanned aerial vehicle) imagery, the author applied ANOVA, the support vector machine (SVM) method, and vegetation indices. The results, which indicated spectral bands and selected vegetation indices, proved that presented approach could be used to differentiate healthy (HEL), non-symptomatic diseased (NSL) and symptomatic diseased (SDL) leaves of pear trees in the orchard.

Despite the extensive amount of research on the application of RS techniques for Fire Blight detection, specific results and recommendations for disease control, particularly for apple trees, are still lacking. Previous research has failed to implement a broad-spectrum range (very few consider the region beyond 1800 nm) and there is no clear indication of the optimum spectral bands for the differentiation of healthy, infected and dry apple tree leaves. Thus, the current study evaluated the application of a wide spectral range (400–2500 nm), including the visible (VIS), near-infrared (NIR) and short-wavelength infrared (SWIR) for the detection of Fire Blight in apple trees, via detailed hyperspectral analysis. Furthermore, the role of RS indices as a tool for the detection of disease symptoms based on hyperspectral data was investigated, and new RS indices were proposed. Lastly, specific narrow spectral bands effective for Fire Blight detection were indicated.

## 2. Materials and Methods

### 2.1. Data Acquisition

Experiments were performed on three groups of leaves: healthy (H), infected (I) and dry (D) (Figure 1). All leaves were at the same stage of development and were collected from apple trees in the quarantine greenhouse at the Institute of Horticulture in Skierniewice (lodzkie, Poland). Leaves of actively growing shoots from young apple trees were infected with *E.amylovora* on August 1st, 2019. These plants were selected, as shoots at this stage of development are much more vulnerable to Fire Blight infection [16–18]. To support the growth of the bacteria, a dedicated growth medium for *E.amylovora* was prepared. Several methods were tested in order to identify the presence of bacteria, including Polymerase Chain Reaction (PCR), which allows for the rapid and precise conformation of bacteria identity [19]. Shoot infection occurred in a quarantine environment with the cutting of shoot tips (right under the first developed leaf) with scissors that were dipped beforehand in the *E.amylovora* aqueous suspension (108 cfu/cc). Leaves were collected from random trees, placed into separate plastic bags and transported under homogeneous cold conditions to a test stand, where spectral signature measurements were performed.



**Figure 1.** Three groups of leaves used for hyperspectral analysis: (a) Healthy (H), (b) dry (D), and (c) infected (I).

### 2.2. Hyperspectral Measurements

Reflectance obtained from laboratory spectroscopic measurements was used for stress detection in plants under quarantine greenhouse conditions. This is a rapid detection method which requires relatively easy sample preparation and is non-invasive [20]. Spectral signatures of leaves were acquired

using two instruments in order to allow for the separate investigation of reflectance (in percent) and spectral resolution for two ranges, the VIS-RedEdge (400–850 nm) range and NIR-SWIR (850–2500 nm) range. The former was measured via the *Evolution 220 Thermo Scientific* laboratory spectrometer using a Xenon Flash Lamp, with a 2-nm spectral resolution. The latter was measured on the *Thermo Scientific iS50NIR* spectrometer equipped with a InGaAs (Indium Gallium Arsenide) sensor and a 0.3-nm resolution. Hyperspectral measurements were performed on 10 healthy (H), 10 dry (D) and a total of 50 infected (I) leaves within five measuring days (August 2nd, 5th, 7th, 9th and 13th). Spectral signatures of dried (D) and healthy (H) leaves were collected on the 2nd of August and used as a reference, while infected (I) leaf signatures were collected on the 2nd, 5th, 7th and 13th day of the disease development. Measurements were performed at the top of the leaf at three locations: Close to the petiole, at the centre of the blade and close to the apex. The raw data from laboratory spectroscopic measurements consisted of approximately 30 spectral signatures of healthy (H), approximately 30 spectral signatures of dry (D) leaves and approximately 150 spectral signatures of infected (I) leaves (30 samples for every measuring day). Spectral signatures were then averaged, resulting in the seven final curves presented in Figures 2–5.

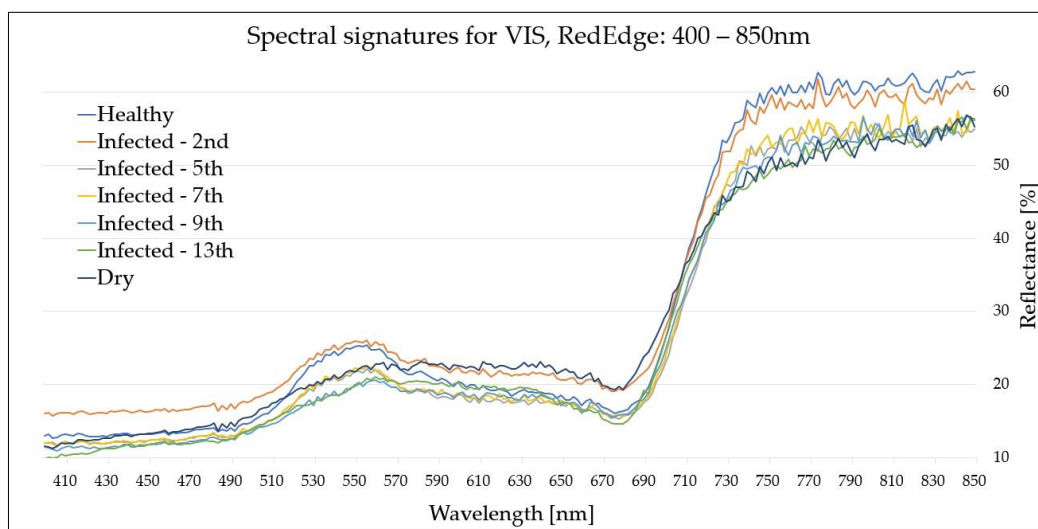


**Figure 2.** Spectral signatures (visible (VIS)-RedEdge region: 400–850 nm) of reference (healthy (H) and dry (D)) and infected (I) leaves from five consecutive measurements performed on the 2nd, 5th, 7th, 9th and 13th August.

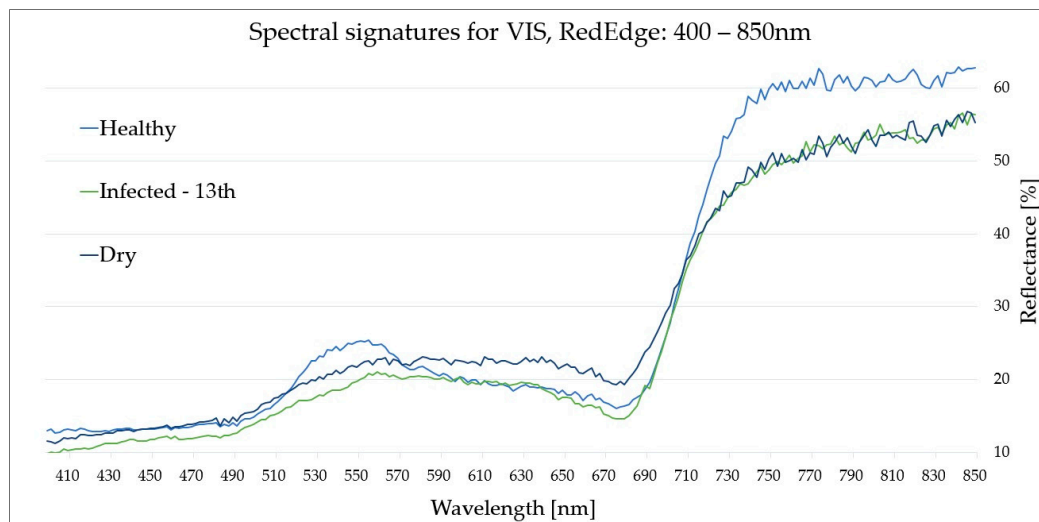


**Figure 3.** Spectral signatures (VIS-RedEdge region: 400–850 nm) of reference (healthy (H) and dry (D)) and infected (I) leaves collected on the 13th August, corresponding to the peak visibility of the disease symptoms.

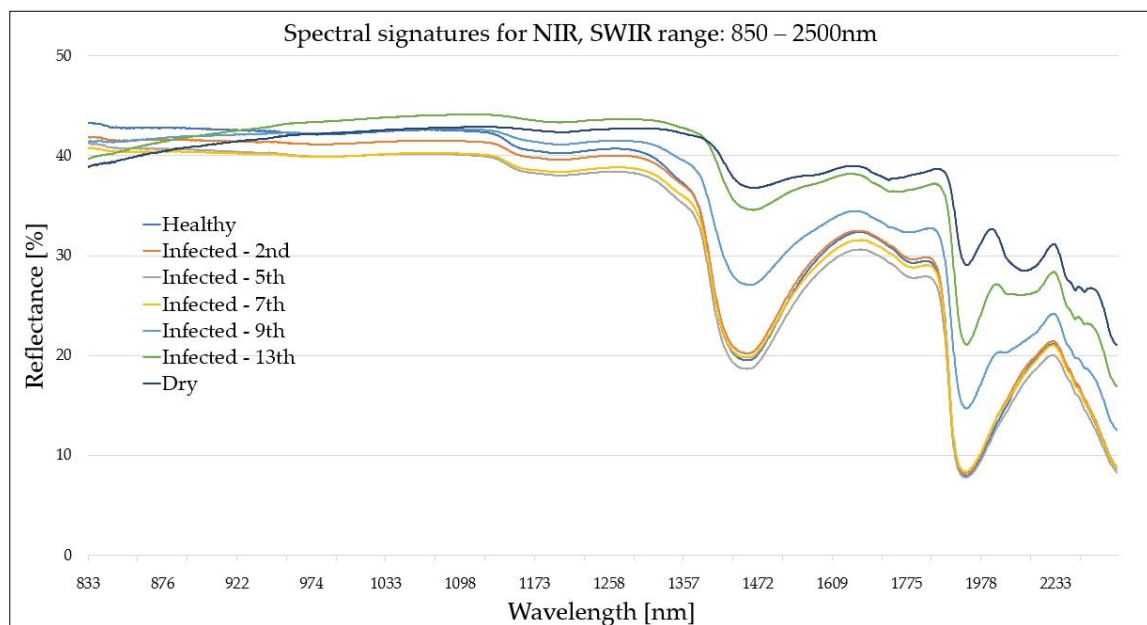


**Figure 4.** Spectral signatures (near-infrared-short-wavelength infrared (NIR-SWIR) region: 850–2500 nm) of reference (healthy (H) and dry (D)) and infected (I) leaves from five consecutive measurements performed on the 2nd, 5th, 7th, 9th and 13th August.

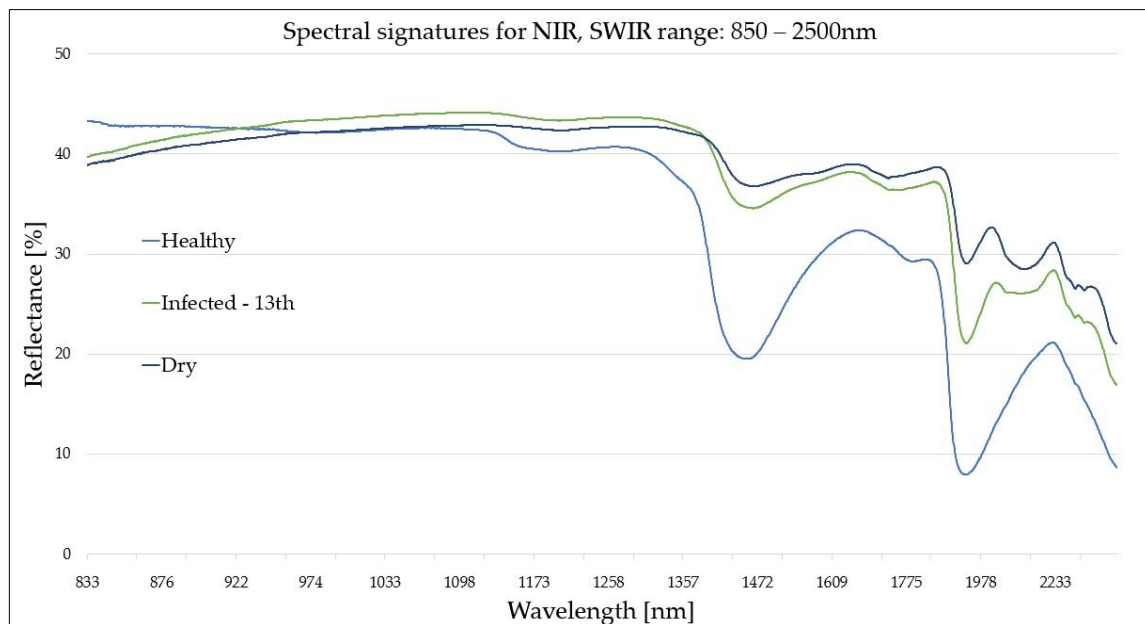


**Figure 5.** Spectral signatures (NIR-SWIR region: 850–2500 nm) of reference (healthy (H) and dry (D)) and infected (I) leaves collected on the 13th August, corresponding to the peak visibility of the disease symptoms.

### 2.3. Hyperspectral Data Analysis

Analysis of variance (ANOVA) was applied to the collected hyperspectral data for a single classification. ANOVA examines the impact of a single classifying factor (divided into multiple levels) on the values of the measurable examined feature. State-of-art ANOVA has been applied, i.e., for the combination of foliar properties of the grapevines with spectral indices [21], classifying diseases and pest types, and differentiating infection levels [22,23]. The statistical method applied in our study is especially similar to Mahlein et al. 2010 [24], where three pathogens of sugar leaves (fungal pathogens *Cercospora beticola*, *Erysiphe betae* and *Uromyces betae*) were detected using spectral signatures and ANOVA analysis with a significance level of  $p = 0.05$ .

In the current study, the classifying factor was the occurrence of the disease (Fire Blight), while the measurable examined feature was the reflectance of apple tree leaves within selected spectral ranges. The input data for the statistical analysis consisted of the reflectance data obtained from spectrometric measurements at the VIS-RedEdge (400–850 nm) and NIR-SWIR (850–2500 nm) regions for healthy (H), infected (I) and dry (D) leaves. The mean reflectance and its variance were calculated at each wavelength (every 2 nm for the VIS-RedEdge region and every 0.3 nm for the NIR-SWIR region) for each group of leaves (H, I and D). ANOVA was used to analyse the differences among group means for the following combinations: Healthy to infected (2nd), healthy to infected (5th), healthy to infected (7th), healthy to infected (9th), healthy to infected (13th) and dry to infected (13th).

Prior to the ANOVA, the homogeneity of variance and normality of reflectance distributions were investigated for each wavelength and group. The influence of disease occurrence on variations in the reflectance value was tested for the confidence intervals of  $p = 0.05$  and  $p = 0.02$ .

## 3. Results

### 3.1. Hyperspectral Measurement Curves

Figures 2 and 3 present the VIS-RedEdge (400–850 nm) spectral signatures obtained from the hyperspectral measurements and used for the subsequent statistical analysis, while Figures 4 and 5 present the equivalent spectral signatures for the NIR-SWIR (850–2500 nm) region. The different coloured curves refer to the spectral signatures of healthy (H), infected (I) and dry (D) leaves.

A comparison of the cumulative average curves revealed characteristic properties of the selected spectral bands. The difference between the signatures of healthy (H) and infected (I) leaves increased with the disease progression, particularly in the green band (500 nm), NIR region (900–1300 nm) (Figures 2 and 3) and at the SWIR water absorption peaks located at 1400 nm and 1900 nm (Figures 4 and 5). Furthermore, the spectral curve of the dry (D) leaves generally coincided with that of the infected (I) leaves within the VIS (400–700 nm) and RedEdge (700 nm) regions. However, an inverse relationship was exhibited between the two leaf groups for the SWIR region due to strong variations at the early stages of disease development. The peaks located at 1400 nm and 1900 nm indicate the most significant differences at the more advanced stage of the disease progression.

The noise in the data that can be spotted in Figures 2 and 3 resulted from the measuring parameters of *Evolution 220 Thermo Scientific* used for the 400–850-nm range. Noise reduction can be achieved, e.g., by applying a longer sample measure time.

Tables 1 and 2 report the ANOVA and statistical analysis results for the VIS-RedEdge (400–850 nm) and NIR-SWIR (850–2500 nm) bands, respectively. The observations were used to evaluate the detection capabilities of specific spectral regions for certain stages of Fire Blight development (starting with apple tree infections on 1st August).

**Table 1.** Comparison of statistical analysis and analysis of variance (ANOVA) results derived from the hyperspectral data collected at the 400–850-nm range.

Samples	Statistically Significant Spectral Bands	One-Way ANOVA Test Observations
H-I (2nd)	770 nm 790 nm 820 nm	Differences between reflectance values of (H) and (I) leaves were insignificant. Minor discrepancies were noticeable around the RedEdge band (770 nm, 790 nm, and 820 nm), however they were not considered effective for Fire Blight detection.
H-I (5th)	~430 nm ~770 nm	(I) leaves exhibited slightly lower reflectance (approx. 1–5%) than those of (H) leaves across the whole signature. A single peak was observed for the visible range in the blue band (~430 nm), showing a 2% difference. The RedEdge exhibited a significant peak at 770 nm with a 5% difference. Discrepancies in the blue band were correlated with a decrease in foliar photosynthetic pigment concentration (chlorophyll <i>a</i> and <i>b</i> ), a typical response for plants under the stress or disease [25]. Reflectance at the RedEdge and beyond was influenced by variations in the leaf structural properties caused by the presence of the pathogen [26].
H-I (7th)	400–450 nm 720–850 nm	Spectral signature of (I) leaves was in strong agreement with the day 5 spectral signature, with reflectance slightly lower (1–5%) than that of the (H) leaves. For the visible range, the blue and blue–green band (400–450 nm) exhibited the greatest discrepancies, with 720–850 nm showing the greatest variation for the RedEdge-NIR region (5–6% lower reflectance for (I) leaves).
H-I (9th)	400–550 nm 700–850 nm	The (I) leaf reflectance decreased on the ninth day from inoculation, with a 5–7% reduction compared to the (H) leaf reflectance. The entire blue (~460 nm) and part of the green (~540 nm) band exhibited the greatest discrepancies within the visible range, while the 700–850-nm region showed the greatest variation within the RedEdge-NIR band. At this stage, the disease development began to have a significant influence on leaf reflectance in the blue, green, RedEdge and NIR regions. This was associated with a greater reduction in chlorophyll and changes in the leaf structural properties.
H-I (13th)	~400 nm ~540 nm 700–850 nm	For strongly developed disease cases, the following bands exhibited the greatest potential for Fire Blight detection: Blue band (~460 nm) with discrepancies (up to 3–4%), strictly correlating with declines in chlorophyll <i>a</i> and <i>b</i> [25]; green band (~540 nm) with discrepancies (up to 5–6%), strictly correlating with a reduction in anthocyanin (vacuolar pigment in plant tissue) absorption [27]; and RedEdge and beyond (700–850 nm), with discrepancies (up to 10%) associated with variations in leaf structural properties [26] and pigment concentrations, particularly the peak at 700 nm [27].
D-I (13th)	~680 nm (only for $p = 0.05$ )	At the confidence interval $p = 0.02$ , the reflectance of (I) leaves with the well-developed disease was in strong agreement with the (D) leaf reflectance. At the confidence interval $p = 0.05$ , a small peak located at ~680 nm exhibited a moderate detection ability, yet the reflectance difference reached only up to 4% for the very narrow band (670–690 nm). Thus, this may be not considered effective for Fire Blight detection. Spectral signatures of (D) and (I) leaves had converging reflectance/absorption features of leaf pigments. Thus, the VIS and RedEdge regions exhibited poor differentiation capabilities for plants with water shortage stress and plants infected with <i>E.amylovora</i> .

**Table 2.** Comparison of statistical analysis and ANOVA results derived from the hyperspectral data collected at the 850–2500-nm range.

Samples	Statistically Significant Spectral Bands	One-Way ANOVA Test Observations
H-I (2nd)	850–1140 nm	(I) leaves exhibited a slightly lower reflectance compared to that of (H) leaves by approximately 1–2%. This was a result of leaf cell structure disturbances due to the presence of the pathogen [26].
H-I (5th)	850–1370 nm and 1650–1850 nm	(I) leaf reflectance was reduced compared to that of the second day of inoculation and was 2–3% lower than the (H) leaf reflectance, with the most significant peak at ~1340 nm.
H-I (7th)	850–1330 nm	(I) leaves exhibited a slightly lower reflectance than the (H) leaves, with the curve trend strongly agreeing with the spectral signature of (I) leaves from the second day. Differences in this region were attributed to cell structure disturbances.
H-I (9th)	~850 nm and 1300–2500 nm	At ~850 nm, (I) exhibited a slightly lower reflectance (~2%) compared to that of the (H) leaves. At the SWIR region, the (I) leaf reflectance was greater than that of the (H) leaves by 3–8%, with the two most significant peaks at ~1430 nm and ~1900 nm. Greater reflectance of (I) leaves at 1430 nm and 1900 nm resulted from the properties of the SWIR region, as reflectance in these two peaks was negatively related to the leaf water content [28].
H-I (13th)	~850 nm and 950–2500 nm	The spectral signatures of (I) and (H) leaves were statistically different (5–15%) across almost the entire course of both curves. The greatest difference (~15%) was located at the ~1440-nm and ~1910-nm water peaks. However, the difference was most evident at the 1910-nm band. The water disturbances in leaves caused by the Fire Blight provided great potential for disease detection at this range. The absorption coefficient of water at the 1440-nm and 1940-nm peaks was 60- and 260-times greater than for the NIR (970 nm) peak, respectively [29].
D-I (13th)	~1450 nm and ~1910 nm	At 850–1400 nm, the differences between reflectance of the (I) and (D) leaves were insignificant statistically. The most evident distinction was observed at the ~1440-nm and ~1910-nm water peaks. This was attributed to variations in leaf water content (despite advanced disease progression, the cells of infected leaves still maintain water content, unlike dry leaves).

### 3.2. Remote Sensing (RS) Indices

Based on the literature detailed in the Introduction, RS indices proved to be effective for Fire Blight detection were calculated in the current study. Table 3 reports the index formulae and visualizes their variability for healthy (H), dry (D) and infected (I) leaves across five consecutive measurement days.

Among the RS indices taken from the literature, the ARI index exhibited a turning point at the seventh day from inoculation, allowing for the discrimination of (I) and (H) leaves. However, this point also corresponded to the convergence of the values for (I) and (D) leaves. RDVI and MTVI1 provided an improved differentiation with disease progression. However, values for (I), (H) and (D) leaves were similar. MSR and NRI exhibited the poorest differentiation between (I) and (H) from the seventh day of infection. Furthermore, peak standard deviation values were observed on day 9 for the majority of the RS indices. This was attributed to the peak in diversity of symptomatic/healthy areas of the leaf blade at this stage of disease development (Figure 6). This was particularly evident for the ARI index, as it is sensitive to plant pigment content (anthocyanin) [30], and disturbances in pigment content are strictly correlated to the plant reaction to the disease [25]. NRI was associated with the highest standard deviation values for current hyperspectral data. Thus, this index was considered to have the poorest performance for the target application. In particular, significant NRI variations

arose from the random selection of (I) leaves with pointwise measurements in three regions. NRI was determined using the green (570 nm) and red (670 nm) bands, and was thus the most sensitive to nitrogen and chlorophyll content disturbances [31].

**Table 3.** Selected remote sensing (RS) index values as a function of disease development. Derived using the measured hyperspectral data.

RS Index and Reference	Formula	RS index Visualization for Infected (I), Healthy (H) and Dry (D) Leaves
<p><b>ARI</b> (Anthocyanin Reflectance Index) Gitelson et al., 2001 [19]</p>	$(R550)^{-1} - (R700)^{-1}$	
<p><b>RDVI</b> (Renormalized Difference Vegetation Index) Haboudane et al., 2004 [20]</p>	$(R800 - R670) / \sqrt{R800 + R670}$	
<p><b>MSR</b> (Modified Simple Ratio) Haboudane et al., 2004 Zarco-Tajada et al., 2005 [20,30]</p>	$(R800/R670 - 1) / \sqrt{R800 - R670 + 1}$	
<p><b>NRI</b> (Nitrogen reflectance index) Devadas et al., 2009 [25]</p>	$(R570 - R670) / (R570 + R670)$	
<p><b>MTVI1</b> (Modified Triangular Vegetation Index 1) Haboudane et al., 2004 [20]</p>	$1,2(1,2(R800 - R550) - 2,5(R670 - R550))$	



**Figure 6.** Infected (I) leaves from the ninth day of HS measurements. Leaf blades were the most diverse in terms of symptomatic/healthy areas occurrence at this stage of disease development.

#### 4. Discussion

The analysis of the spectral signatures at specific stages of Fire Blight development provides information on the most promising spectral bands for disease detection and the differentiation of healthy (H), infected (I) and dry (D) leaves.

For the VIS-RedEdge (400–850 nm) range, as the disease progressed, the reflectance of the infected (I) leaves was reduced, particularly in the blue (~460 nm), green (~540 nm) and RedEdge (~750 nm) bands, with discrepancies reaching 3–4%, 5–6% and 10% (the most significant), respectively. Thus, this region was demonstrated to be effective for Fire Blight detection following the seventh day from inoculation. However, the VIS-RedEdge region was not able to effectively distinguish between (I) and (D) leaves due to highly similar reflectance values, particularly from the fifth day from inoculation.

For the NIR-SWIR (850–2500 nm) region, as the disease progressed, the (I) leaf reflectance at 1370–2500 nm increased (and was strictly correlated with water content). However, at approximately 1000 nm, the (I) leaves exhibited a reduction in reflectance. A single narrow spectral band from the SWIR region (1450 nm) exhibited strong potential in the differentiation of (H) and (I) leaves. However, it failed to distinguish between (I) and (D) samples. The 1900-nm band exhibited the best differentiation between all three leaf groups across a whole spectral range (400–2500 nm). In general, the NIR-SWIR region proves to be effective in the differentiation of all three leaf groups due to the water absorption peaks located at ~1450 nm and ~1910 nm.

The majority of the RS indices proposed in the literature were derived using the VIS and NIR bands. Furthermore, our results indicate that the spectral signatures of leaves at these bands did not differ significantly (with the exception of ARI). Thus, we propose two new vegetation indices, namely QFI 1450 (1600–1450)/(1600 + 1450 nm) and QFI 1910 (1600–1910)/(1600 + 1910 nm), presented in Figures 7 and 8 using the collected hyperspectral data, respectively. Both of the new RS indices were able to differentiate infected (I) and healthy (H) leaves of apple trees. In addition, the QFI 1910 index differentiated infected (I) and dry (D) leaves, and thus proves to be the most effective for Fire Blight detection. The proposed indices were proved to be optimal in terms of disease detection due to their relationship with leaf water content, which plays a significant role in infection development.

Two new vegetation indices, namely QFI 1450 and QFI 1910, were constructed by selecting two groups of wavelengths:

G1: For which the occurrence of disease has a statistically significant impact on the reflectance value, allowing the differentiation healthy, dry and infected leaves.

G0: For which the reflectance value of all three groups of leaves (healthy, dry and infected) are statistically undistinguishable.

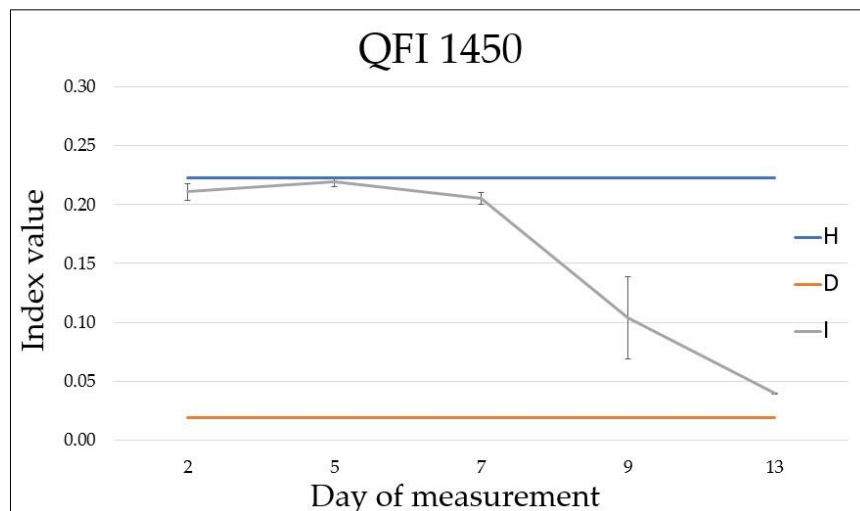


**Figure 7.** QFI 1450 index  $(1600-1450)/(1600 + 1450 \text{ nm})$ . The index was able to differentiate between infected (I) and healthy (H) leaves following the seventh day from plant inoculation.

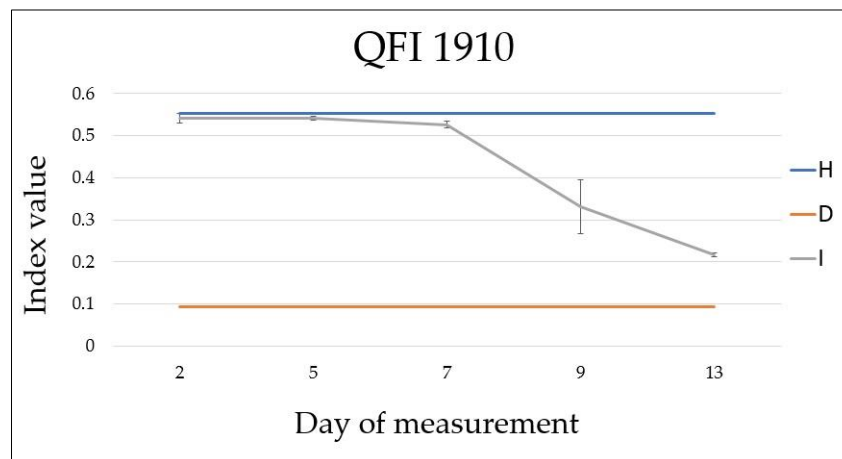


**Figure 8.** QFI 1910 index  $(1600-1910)/(1600 + 1910 \text{ nm})$ . The index was able to differentiate between infected (I), healthy (H) leaves, and dry (D) leaves following the seventh day from plant inoculation.

Based on G0 and G1, new spectral indices were constructed according to the standard method of constructing normalized differential indices, which was first used by Rouse et al. 1973 [32]:

$$QFI = (g_0 - g_1)/(g_0 + g_1), \text{ where } g_0 \in G_0 \text{ and } g_1 \in G_1.$$

QFI 1450 and QFI 1910 can be validated by spectral field measurements using portable spectroradiometer or by the analysis of high-resolution hyperspectral imagery obtained by ground and/or airborne sensors.

Table 4 reports the Pearson correlation between the RS values in terms of infection progress (Table 4). The infection progress values were set proportionally to the development of the pathogen, with the value of the first day set as 0% and that of the last day as 100%. Results demonstrate that the strongest positive correlation with the development of the disease was associated with ARI and MSR indices. The strongest negative correlation was associated with QFI 1450 and QFI 1910. These correlations correspond to the highest absolute values. Thus, we conclude that the QFI 1450 and QFI 1910 indices exhibited the strongest relationship with the disease development. The *p-values* (Table 4.) show that the results are statistically significant. The alpha value of 0.05 was used for calculations.

**Table 4.** Pearson correlation between different RS indices. *p-values* are presented at the inverse matrix of the correlation values.

$\rho$	ARI	RDVI	MSR	NRI	MTVII	QFI 1450	QFI 1910	Infection Progress
<b>ARI</b>		0.00000005	0.00000177	0.00007404	0.00000176	0.01661837	0.00347132	0.00047368
<b>RDVI</b>	0.244		0.00000006	0.00000005	0.00000226	0.00000026	0.00000130	0.00000016
<b>MSR</b>	0.568	0.621		0.00000210	0.00000194	0.00006976	0.00137624	0.00016507
<b>NRI</b>	0.468	0.304	0.625		0.00000177	0.03614596	0.01099716	0.00089811
<b>MTVII</b>	−0.611	0.716	0.471	0.116		0.00000167	0.00000161	0.00000002
<b>QFI 1450</b>	−0.997	−0.221	−0.544	−0.507	0.484		0.00088589	0.00175866
<b>QFI 1910</b>	−0.997	−0.251	−0.522	−0.494	0.506	0.999		0.00789725
<b>Infection Progress</b>	0.895	0.449	0.874	0.520	−0.633	−0.903	−0.910	

A strong inverse relationship was revealed between ARI and QFI 1450 (and QFI 1910). This was linked to the water absorption and anthocyanins, as anthocyanin content was represented in the ARI index. The Fire Blight-induced water deficits increased with anthocyanin content per plant. This suggests that the minimum values of both QFIs indicated the lowest water leaf content, while maximum ARI values were related to maximum anthocyanin amounts in leaves. Furthermore, anthocyanins may be produced as a part of a plant's response to stress. This result is in accordance with Saure [33], Leng et al. [34], Merzlyak and Chivunkova [35], Feild [36], Roby et al. [37] and Chalker–Scott [38].

Although MSR exhibited a strong correlation with the infection progress, its correlation with the new indices was weak. This was due to the lack of connection between water absorbance (represented by the QFI indices) and chlorophyll concentration (indirectly represented by MSR). This may suggest that chlorophyll content decreased during the infection progress. However, its correspondence to leaf water content was lacking. Much research has investigated the role of chlorophyll content in spectral indices, including Main et al. [39] and Gitelson and Merzlyak [40,41].

## 5. Conclusions

Our study demonstrates that hyperspectral analysis across a wide spectral range (400–2500 nm) allows for the identification of reflectance variability in apple tree leaves infected by *E.amylovora*. Experimental results prove that this approach can differentiate between infected (I), healthy (H) and dry (D) leaves. Thus, this method is applicable for Fire Blight detection and can be adopted by authorities, researchers and breeders for disease management. The more advanced the development of the Fire Blight, the more significant the differences in the spectral signatures of healthy, infected and dry leaves. Hence, the disease detection proves to be easier as the infection progresses.

Further developments of the proposed method should be based on indicated spectral bands to allow for the direct detection and monitoring of diseases in orchards via suitable imaging sensors and a carrying platform.

Two new proposed indices determined as the QFI1450 index  $(1600-1450)/(1600 + 1450 \text{ nm})$  and the QFI1910 index  $(1600-1910)/(1600 + 1910 \text{ nm})$  can be employed for the real-time (or near real-time) automatic detection of *E. amylovora* infection across different disease progression stages.

Hyperspectral analysis, with its undeniable advantages (e.g., non-invasive, real-time results and does not require sample preparation) proved to be effective for Fire Blight detection and can be expanded and scaled to other plants and pathogens.

The strongest (negative) Pearson correlation between infection progress and the RS indices was observed with QFI 1450 and QFI 1910, which were strictly related to the leaf water content. In addition, ARI and MSR can be applied for leaf observations across time. In particular, ARI is related to anthocyanins and pigment content, while MSR is related to chlorophyll content.

Current dynamic developments in the fields of sensors, IoT (Internet of Things) and UAVs (Unmanned Aerial Vehicles) provide ample opportunities for the further evolution of the proposed

method in field conditions. Target users include plant health and seed field inspectors, who can adapt our method to their duties with regard to the real-time and automatic detection of infected plants in orchards and orchard tree nurseries.

**Author Contributions:** Conceptualization, H.S. and K.K.; Data curation, M.S.; Formal analysis, M.S.; Investigation, H.S. and K.K.; Methodology, H.S., K.K., A.M. and J.P.; Project administration, H.S.; Resources, K.K., M.S., A.M. and J.P.; Software, J.K.; Supervision, H.S.; Validation, H.S., K.K. and J.K.; Visualization, H.S. and M.S.; Writing—original draft, H.S.; Writing—review & editing, K.K. and J.K. All authors have read and agreed to the published version of the manuscript.

**Funding:** Studies described in this paper were performed in August 2019, within Task 2 of the FITOEXPORT Project (Gospostrateg1/385957/5/NCBR/2018), financed from the National Center for Research and Development. Primary recipients of the project results are orchardmen, growers and field inspectors of the Main Inspectorate of Plant Health and Seed Inspection, who are obliged to conduct regular orchard inspections, at registered areas, targeted at Fire Blight detection.

**Acknowledgments:** We thank the Institute of Horticulture in Skierniewice for fruitful cooperation and the possibility to conduct measurements on tree samples in a quarantine greenhouse environment, the Main Inspectorate of Plant Health and Seed Inspection for their valuable input and all members of the FITOEXPORT Project team.

**Conflicts of Interest:** The authors declare no conflict of interest.

## References

1. Radunovic, D.; Gavrilovic, V.; Gasic, K.; Krstic, M. Monitoring of *Erwinia amylovora* in Montenegro. *Pestic. Fitomedicina* **2015**, *30*, 179–185. [[CrossRef](#)]
2. Paulin, J.-P. Control of Fireblight in European Pome Fruits. *Outlook Agric.* **1996**, *25*, 49–55. [[CrossRef](#)]
3. Gaucher, M.; Dugé de Bernonville, T.; Guyot, S.; Dat, J.F.; Brisset, M.N. Same ammo, different weapons: Enzymatic extracts from two apple genotypes with contrasted susceptibilities to fire blight (*Erwinia amylovora*) differentially convert phloridzin and phloretin invitro. *Plant Physiol. Biochem.* **2013**, *72*, 178–189. [[CrossRef](#)]
4. Shtienberg, D.; Manulis-Sasson, S.; Zilberstaine, M.; Oppenheim, D.; Shwartz, H. The Incessant Battle Against Fire Blight in Pears: 30 Years of Challenges and Successes in Managing the Disease in Israel. *Plant Dis.* **2015**, *99*, 1048–1058. [[CrossRef](#)]
5. Cother, E. Fire Blight: The Disease and its Causative Agent, *Erwinia amylovora*. Ed. J. Vanneste. *Australas. Plant Pathol.* **2001**, *30*, 77. [[CrossRef](#)]
6. McManus, P.S.; Stockwell, V.O.; Sundin, G.W.; Jones, A.L. Antibiotic Use In Plant Agriculture. *Annu. Rev. Phytopathol.* **2002**, *40*, 443–465. [[CrossRef](#)]
7. Broggini, G.A.L.; Duffy, B.; Holliger, E.; Schärer, H.J.; Gessler, C.; Patocchi, A. Detection of the fire blight biocontrol agent *Bacillus subtilis* BD170 (Biopro®) in a Swiss apple orchard. *Eur. J. Plant Pathol.* **2005**, *111*, 93–100. [[CrossRef](#)]
8. Van Der Zwet, T.; Beer, S.V. *Fire Blight—Its Nature, Prevention, and Control: A Practical Guide to Integrated Disease Management*; U.S. Dept. of Agriculture: Washington, DC, USA, 1999.
9. Bagheri, N.; Mohamadi-Monavar, H.; Azizi, A.; Ghasemi, A. Detection of Fire Blight disease in pear trees by hyperspectral data. *Eur. J. Remote Sens.* **2018**, *51*, 1–10. [[CrossRef](#)]
10. Alnaasan, Y. Hyperspectral Discrimination of Fire Blight Infection in Apple and Pear, and Molecular Typing of Some Mediterranean Isolates of Its Causal Agent *Erwinia Amylovora*. Ph.D. Thesis, Department of Agriculture, Forestry, Nature, Energy Science and Technology (DAFNE), Tuscia University, Viterbo, Italy, 2015.
11. Jarolmasjed, S.; Sankaran, S.; Marzougui, A.; Kostick, S.; Si, Y.; Quirós Vargas, J.J.; Evans, K. High-Throughput Phenotyping of Fire Blight Disease Symptoms Using Sensing Techniques in Apple. *Front. Plant Sci.* **2019**, *10*, 576. [[CrossRef](#)] [[PubMed](#)]
12. Singh, B.; Singh, M.; Singh, G.; Suri, K.; Pannu, P.P.S.; Bal, S.K. *Hyper-Spectral Data for the Detection of Rice Bacterial Leaf Blight (BLB) Disease*; AIPA: Jakarta, Indonesia, 2012.
13. Zhang, M.; Qin, Z. Spectral analysis of tomato late blight infections for remote sensing of tomato disease stress in California. In Proceedings of the International Geoscience and Remote Sensing Symposium (IGARSS), Anchorage, AK, USA, 20–24 September 2004; Volume 6, pp. 4091–4094.

14. Rizzuti, A.; Aguilera-Sáez, L.M.; Santoro, F.; Valentini, F.; Gualano, S.N.; D'Onghia, A.M.; Gallo, V.; Mastrorilli, P.; Latronico, M. Detection of *Erwinia amylovora* in pear leaves using a combined approach by hyperspectral reflectance and nuclear magnetic resonance spectroscopy. *Phytopathol. Mediterr.* **2018**, *57*, 296–306.
15. Bagheri, N. Application of aerial remote sensing technology for detection of fire blight infected pear trees. *Comput. Electron. Agric.* **2020**, *168*, 105147. [[CrossRef](#)]
16. Ozrenk, K.; Balta, F.; Çelik, F. Levels of fire blight (*Erwinia amylovora*) susceptibility of native apple, pear and quince germplasm from Lake Van Basin, Turkey. *Eur. J. Plant Pathol.* **2012**, *132*, 229–236. [[CrossRef](#)]
17. Hepaksoy, S.; Unal, A.; Can, H.Z.; Saygili, H.; Türküsay, H. Distribution of fire blight (*Erwinia amylovora* (Burrill) winslow et al.) disease in western anatolia region in Turkey. *Acta Hort.* **1999**, *489*, 193–195. [[CrossRef](#)]
18. Byers, R.E.; Yoder, K.S. The Effect of BAS-125W on Apple Tree Growth, Fruit Quality, and Fireblight Suppression. *HortScience* **1997**, *32*, 557. [[CrossRef](#)]
19. Kałużna, M.; Puławska, J.; Mikciński, A. Evaluation of methods for *erwinia amylovora* detection. *J. Hortic. Res.* **2014**, *21*, 65–71. [[CrossRef](#)]
20. Sankaran, S.; Ehsani, R. Visible–near infrared spectroscopy based citrus greening detection: Evaluation of spectral feature extraction techniques. *Crop Prot.* **2011**, *30*, 1508–1513. [[CrossRef](#)]
21. Maimaitiyiming, M.; Miller, A.; Ghulam, A. Discriminating Spectral Signatures Among and Within Two Closely Related Grapevine Species. *Photogramm. Eng. Remote Sens.* **2016**, *82*, 51–62. [[CrossRef](#)]
22. Yuan, L.; Zhang, J.; Shi, Y.; Nie, C.; Wei, L.; Wang, J. Damage Mapping of Powdery Mildew in Winter Wheat with High-Resolution Satellite Image. *Remote Sens.* **2014**, *6*, 3611–3623. [[CrossRef](#)]
23. Zhang, J.; Pu, R.; Wang, J.; Huang, W.; Yuan, L.; Luo, J. Detecting powdery mildew of winter wheat using leaf level hyperspectral measurements. *Comput. Electron. Agric.* **2012**, *85*, 13–23. [[CrossRef](#)]
24. Mahlein, A.; Steiner, U.; Dehne, H.; Oerke, E. Spectral signatures of sugar beet leaves for the detection and differentiation of diseases. *Precis. Agric.* **2010**, *11*, 413–431. [[CrossRef](#)]
25. Boquera, L.E.; Lobit, P.; Morales, V.C. Leaf chlorophyll content estimation in the Monarch Butterfly Biosphere Reserve. *Rev. Fitotec. Mex.* **2010**, *33*, 175–181.
26. Barton, C.V.M. Advances in remote sensing of plant stress. *Plant Soil* **2012**, *354*, 41–44. [[CrossRef](#)]
27. Gitelson, A.; Merzlyak, M. *Non-Destructive Assessment of Chlorophyll Carotenoid and Anthocyanin Content in Higher Plant Leaves: Principles and Algorithms*; University of Nebraska-Lincoln: Lincoln, NE, USA, 2004.
28. Yilmaz, M.T.; Hunt, E.R.; Jackson, T.J. Remote sensing of vegetation water content from equivalent water thickness using satellite imagery. *Remote Sens. Environ.* **2008**, *112*, 2514–2522. [[CrossRef](#)]
29. Wilson, R.H.; Nadeau, K.P.; Jaworski, F.B.; Tromberg, B.J.; Durkin, A.J. Review of short-wave infrared spectroscopy and imaging methods for biological tissue characterization. *J. Biomed. Opt.* **2015**, *20*, 030901. [[CrossRef](#)]
30. Gitelson, A.A.; Merzlyak, M.N.; Chivkunova, O.B. Optical Properties and Nondestructive Estimation of Anthocyanin Content in Plant Leaves. *Photochem. Photobiol.* **2001**, *74*, 38. [[CrossRef](#)]
31. Devadas, R.; Lamb, D.W.; Simpfendorfer, S.; Backhouse, D. Evaluating ten spectral vegetation indices for identifying rust infection in individual wheat leaves. *Precis. Agric.* **2009**, *10*, 459–470. [[CrossRef](#)]
32. Rouse, J.W.; Haas, R.H.; Deering, D.W.; Schell, J.A.; Harlan, J. *Monitoring the Vernal Advancement and Retrogradation (Green Wave Effect) of Natural Vegetation*. [*Great Plains Corridor*]; Remote Sensing Center, Texas A&M University: College Station, TX, USA, 1973.
33. Saure, M.C. External control of anthocyanin formation in apple. *Sci. Hortic. (Amsterdam)* **1990**, *42*, 181–218. [[CrossRef](#)]
34. Leng, P.; Itamura, H.; Yamamura, H.; Deng, X.M. Anthocyanin accumulation in apple and peach shoots during cold acclimation. *Sci. Hortic. (Amsterdam)* **2000**, *83*, 43–50. [[CrossRef](#)]
35. Merzlyak, M.N.; Chivkunova, O.B. Light–stress–induced pigment changes and evidence for anthocyanin photoprotection in apples. *J. Photochem. Photobiol. B Biol.* **2000**, *55*, 155–163. [[CrossRef](#)]
36. Feild, T.S.; Lee, D.W.; Holbrook, N.M. Why leaves turn red in autumn. The role of anthocyanins in senescing leaves of red–osier dogwood. *Plant Physiol.* **2001**, *127*, 566–574. [[CrossRef](#)]
37. Roby, G.; Harbertson, J.F.; Adams Douglas, A.; Matthews, M.A. Berry size and vine water deficits as factors in winegrape composition: Anthocyanins and tannins. *Aust. J. Grape Wine Res.* **2004**, *10*, 100–107. [[CrossRef](#)]

38. Chalker–Scott, L. Environmental Significance of Anthocyanins in Plant Stress Responses. *Photochem. Photobiol.* **1999**, *70*, 1–9. [[CrossRef](#)]
39. Main, R.; Cho, M.A.; Mathieu, R.; O’Kennedy, M.M.; Ramoelo, A.; Koch, S. An investigation into robust spectral indices for leaf chlorophyll estimation. *ISPRS J. Photogramm. Remote Sens.* **2011**, *66*, 751–761. [[CrossRef](#)]
40. Gitelson, A.A.; Merzlyak, M.N. Signature analysis of leaf reflectance spectra: Algorithm development for remote sensing of chlorophyll. *J. Plant Physiol.* **1996**, *148*, 494–500. [[CrossRef](#)]
41. Gitelson, A.A.; Merzlyak, M.N. Remote sensing of chlorophyll concentration in higher plant leaves. *Adv. Sp. Res.* **1998**, *22*, 689–692. [[CrossRef](#)]



© 2020 by the authors. Licensee MDPI, Basel, Switzerland. This article is an open access article distributed under the terms and conditions of the Creative Commons Attribution (CC BY) license (<http://creativecommons.org/licenses/by/4.0/>).